Helicopter flight characteristics in icing conditions

Yihua Cao **Guozhi Li**
yihuacs@yahoo.com.cn
Department of Aircraft Engineering
Beijing University of Aeronautics and Astronautics
Beijing, China

R. A. Hess
Department of Mechanical and Aerospace Engineering
University of California, Davis
California, USA

ABSTRACT

A method to predict the effects of rotor icing on the flight characteristics of a UH-60A helicopter is presented. By considering both natural ice shedding and different types of ice accretion due to local temperature variations on the blade surface, an improved rotor icing model was developed. Next, the effects of icing on rotor force, torque and flapping were incorporated in a nonlinear helicopter dynamic model. Based upon icing design envelopes in cumuliform clouds, trim and stability characteristics were studied. Further development of the helicopter state-space model allowed control and handling qualities characteristics to be investigated with variation of the three icing-related cloud variables (atmospheric temperature, liquid water content, and median volumetric diameter). Results indicated that this method of evaluating rotorcraft icing is both feasible and useful.

NOMENCLATURE

a_s	slope of rotor-blade lift curve per radian, 1/rad
a_0, a_{1s}, b_{1s}	ice-free rotor flapping coefficients, deg
a_0^i, a_{1s}^i, b_{1s}^i	iced rotor flapping coefficients, deg
A,B,C,D	plant matrix, control distribution matrix, output matrix, and carry through matrix*n*,
C, C', ΔC	ice-free/iced coefficient, increments of C due to icing

Paper No. 3641. Manuscript received 21 October 2010, revised version received 2 June 2011, second revision received 22 August 2011, accepted 11 November 2011.

https://doi.org/10.1017/S0001924000007375 Published online by Cambridge University Press

g	gravitational acceleration, N/kg
HE	cloud horizontal extent, nmi
I	helicopter product of inertial, kg/m^2
L, M, N	rolling, pitching, and yawing angular acceleration, rad/s^2
LWC	liquid water content, g/m^3
n,m	station number along the blade-spanwise and azimuthal sector number of the rotor disk
MWD	median volumetric diameter, μm
p, q, r	angular rate of helicopter along body x-axis, y-axis, and z-axis, respectively, rad/s
q_{pk}	peak pitch rate, deg/s
$\overline{r}$, M, μ	nondimensional of r by rotor radius, and Mach number, and rotor advance ratio
T_C, T_C^{GL}, T_C^R	local temperature, and glaze/rime ice boundary local temperature on blade surface, ºC
T_S, T_{GL}, T_R	atmospheric temperature, and glaze/rime ice boundary atmospheric temperature, ºC
u, v, w	velocity of helicopter along body x-axis, y-axis, and z-axis, ms^{-1}
$\overline{u}_t$, $\overline{u}_p$	relative wind velocity from forward flight and upward flapping at blade section
$w_{1\cdot5}$	index of vertical axis control power, ms^{-1}
X, Y, Z	linear acceleration in the body x-axis, y-axis, and z-axis direction, m/s^2
X,Y,U	state vector, output vector, and input vector
$\dot{X}$	helicopter velocity along inertial x-axis, knots
α	aerofoil angle-of-attack, deg
δ	control deflection, cm
$\Delta\theta_{pk}$, $\Delta\theta_{min}$	pitch attitude change, and minimum pitch attitude change, deg
γ_{air}, r_T	ratio of specific heats, and boundary-layer recovery factor
θ, ϕ, ψ	pitching, rolling, and yawing attitude angle, deg
σ, γ	rotor solidity, and rotor blade lock number
τ	icing time, min
Ω	rotor rotational speed, rad/s
ψ, β, β′	rotor blade azimuth angle, and ice-free/iced flapping angle, deg

Subscripts

L, D	lift, and drag
T, Y, H, Q	rotor thrust, side-force, horizontal force, and rotor torque
Max, 0	maximum value, and trim condition
B,C, S, R	longitudinal, collective, lateral, and directional control stick
xz, xx, zz	xz-plane, x-axis, and z-axis

1.0 INTRODUCTION

Degraded weather conditions involving rain, snow, ice, and frost are frequently encountered in helicopter flight in an altitude range from sea level to 6,000m. The hazards associated with ice accretion in such conditions should be considered as atmospheric liquid water content increases. Rotor blade ice accretion, which primarily affects rotor blade aerodynamic characteristics, degrades performance and flying qualities and can pose a threat to flight safety.

Within the past 30 years, researchers have drawn upon experimental and theoretical research

https://doi.org/10.1017/S0001924000007375 Published online by Cambridge University Press

involving fixed-wing and propeller icing to investigate the potentially hazardous effects of ice accretion on rotor blades[1-6]. Korkan *et al*[5-7] and Flemming *et al*[8, 9] initially studied rotorcraft icing problems, but only as regards the effects of icing on rotor blade aerodynamics and rotor torque. More recently, Flemming and Lusczz[10] incorporated an empirical icing code in a flight simulator to predict the effect of ice accretion on aircraft flight dynamics in trimmed and maneuvering flight. No flight test data was available to verify the accuracy of the model. At present, the flight dynamic characteristics of a tandem-rotor helicopter in rotor icing conditions[11] has been investigated but only including the effects of rime ice accretion.

Helicopter icing simulation methods can be divided into experimental and computational studies, with the latter involving computational fluid dynamics (CFD) tools. Experimental studies can be used to obtain data using icing wind tunnel facilities and other man-made icing environments[12-15]. Few detailed studies on the flight characteristics of full-scale helicopters in icing conditions have been undertaken because of high cost, high risk, and the requirement for long-duration icing tests. Thus, the experimental approach may not be economical, safe or practical for studying the helicopter icing problem. CFD simulation can be considered as an effective means of augmenting experimental studies[16]. Indeed, many such computational tools have been successfully developed, for example, LEWICE[17], ONERA 2-3D/3-D[18], IMPIN3D[19], and FENSAP-ICE[20]. Because of variable airflow velocities and angles of attack on arbitrary rotor radial and azimuth locations, employing numerical simulation of helicopter rotor icing is considerably more complex than that for fixed-wing icing studies. Such studies can, however, provide theoretical insight into the mechanism of rotor icing.

The current study combines available two-dimensional airfoil icing data from wind tunnel studies, a nonlinear helicopter dynamic model, and a linear helicopter dynamic state-space model to develop a method to analyse the effects of rotor icing on the flight dynamic characteristics of a UH-60A single-rotor helicopter. An engineering rotor icing model is first established. Then, a nonlinear helicopter dynamic model is created that includes the effects of a rotor icing encounter. Based upon icing design envelopes in cumuliform clouds[21], trim and stability characteristics are studied for forward flight. A linear helicopter state-space model is then developed that allows specification documents such as MIL-F-83300[22] and ADS-33E-PRF[23] to be used to characterise control characteristics, attitude quickness, interaxis coupling, and vertical axis control power as a function of icing time, atmospheric temperature, liquid water content, and median volumetric diameter.

2.0 MODEL REPRESENTATION

2.1 Rotor icing model

Introducing averaging methodology[5], the rotor disk can be divided into $n \times m$ calculation sectors, with n stations along the blade-spanwise direction for each of the m azimuth sectors. By analysing the rotor blade airfoil ice accretion in each calculation sector and summing effects over all of the sectors, a rotor icing model can be established. This is accomplished considering natural ice shedding and local temperature variations on the blade surface.

Details about the ice shedding model can be found in Ref. 11. In this paper, further studies on different types of ice accretion due to local temperature variations on the blade surface are mainly discussed. The local temperature T_C on the rotor blade surface is a function of atmospheric temperature, local angle-of-attack, and local Mach number[8].

https://doi.org/10.1017/S0001924000007375 Published online by Cambridge University Press

$$T_C = (T_S + 273\cdot15(1+\frac{\gamma_{air}-1}{2}r_T\mathrm{M}^2) + 0\cdot33(\alpha-6) - 273\cdot15 \quad \ldots(1)$$

When, $T_C < 0$ºC ice accretion occurs on the rotor blade. And as T_C decreases from zero to T_C^{GL} to T_C^R ,and then to the temperature that even lower than T_C^R, the accreted ice shape on the outer portion of the rotor blade changes from beak to glaze to mixed, and to rime ice[24]. The glaze and rime ice boundary atmospheric temperature[8] on the blade surface are

$$T_{GL} = \frac{273\cdot15 - 0\cdot33(\alpha-6)}{1+\frac{\gamma_{air}-1}{2}r_T\mathrm{M}^2} - 0\cdot33\alpha - 273\cdot15 \quad \ldots(2)$$

$$T_R = (224\cdot79\cdot LWC^2 - 326\cdot25\cdot LWC + 35\cdot59)\mathrm{M}^2 + (-83\cdot05\cdot LWC^2 + 57\cdot73\cdot LWC - 26\cdot38)\mathrm{M} \quad \ldots(3)$$

So combining with formula (1), (2), and (3), T_C^{GL} and T_C^R can be further deduced as

$$T_C^{GL} = -0\cdot33\alpha(1+\frac{\gamma_{air}-1}{2}r_T\mathrm{M}^2) \quad \ldots(4)$$

$$T_C^R = (T_R + 273\cdot15(1+\frac{\gamma_{air}-1}{2}r_T\mathrm{M}^2) + 0\cdot33(\alpha-6) - 273\cdot15 \quad \ldots(5)$$

Corresponding ΔC_L and ΔC_D of the rime and glaze/beak ice can be calculated by using the empirical correlation of Flemming[24]. And the empirical correlation of the mixed ice can be conducted as referred to in Ref. 8.

Nevertheless, once $T_C \geq 0$ºC, icing will not occur and the calculations are not undertaken. The iced lift/drag coefficient of the rotor blade aerofoil can be written as

$$C_L^{'} = (1+\Delta C_L / C_L)C_L \quad \ldots(6)$$

$$C_D^{'} = (1+\Delta C_D / C_D)C_D \quad \ldots(7)$$

2.2 Flight dynamic model

Employing theoretical considerations (helicopter rotor vortex, element, and momentum theory[25]) and introducing the methodology for establishing tandem rotor helicopter flight dynamic model[26], an ice-free single rotor helicopter flight dynamic model can be developed. Previous icing study work[11] involves introducing the increments of rotor thrust, side force, horizontal force, and torque coefficients into the ice-free flight dynamic model. Those increments of coefficients are

$$\Delta C_T^{'} = \frac{\sigma}{4\pi}\int_0^{2\pi}\int_0^1 \bar{u}_t^2 \Delta C_L \mathrm{d}\bar{r}\mathrm{d}\psi \quad \ldots(8)$$

$$\Delta C_Y^{'} = -\frac{\sigma}{4\pi}\int_0^{2\pi}\int_0^1 [(\bar{u}_t^2\Delta C_D - \bar{u}_t\bar{u}_p\Delta C_L)\mathrm{Cos}\psi - \bar{u}_t^2\Delta C_L\beta\mathrm{Sin}\psi]\mathrm{d}\bar{r}\mathrm{d}\psi \quad \ldots(9)$$

https://doi.org/10.1017/S0001924000007375 Published online by Cambridge University Press

$$\Delta C_H' = \frac{\sigma}{2\pi}\int_0^{2\pi}\int_0^1 [(\bar{u}_t^2 \Delta C_D - \bar{u}_t \bar{u}_p \Delta C_L)\mathrm{Sin}\psi - \bar{u}_t^2 \Delta C_L \beta \mathrm{Cos}\psi]\mathrm{d}\bar{r}\mathrm{d}\psi \quad \ldots (10)$$

$$\Delta C_Q' = \frac{\sigma}{2\pi}\int_0^{2\pi}\int_0^1 (\bar{u}_t^2 \Delta C_D - \bar{u}_t \bar{u}_p \Delta C_L)\bar{r}\mathrm{d}\bar{r}\mathrm{d}\psi \quad \ldots (11)$$

Coefficients of rotor thrust, side force, horizontal force, and torque due to icing can be deduced as

$$\begin{cases} C_T' = C_T + \Delta C_T' \\ C_Y' = C_Y + \Delta C_Y' \\ C_H' = C_H + \Delta C_H' \\ C_Q' = C_Q + \Delta C_Q' \end{cases} \quad \ldots (12)$$

Previous work does not consider the effect on rotor flapping model due to actual rotor icing. In this paper, to improve the fidelity of the iced flight dynamic model, further studies on considering ice increment changes in the coning of the rotor and in the first-order longitudinal/lateral flapping coefficients are conducted

$$\Delta a_0' = \frac{\gamma}{2\pi a_S}\int_{-\pi}^{\pi}\int_0^1 \bar{u}_t^2 \Delta C_L \bar{r}\mathrm{d}\bar{r}\mathrm{d}\psi \quad \ldots (13)$$

$$\Delta a_{1s}' = -\frac{4}{\pi(1-\frac{\mu^2}{2})a_S}\int_{-\pi}^{\pi}\int_0^1 \bar{u}_t^2 \Delta C_L \bar{r}\mathrm{Sin}\psi\mathrm{d}\bar{r}\mathrm{d}\psi \quad \ldots (14)$$

$$\Delta b_{1s}' = \frac{4}{\pi(1+\frac{\mu^2}{2})a_S}\int_{-\pi}^{\pi}\int_0^1 \bar{u}_t^2 \Delta C_L \bar{r}\mathrm{Cos}\psi\mathrm{d}\bar{r}\mathrm{d}\psi \quad \ldots (15)$$

The corresponding iced-rotor flapping model in Fourier series form can be established as

$$\begin{cases} a_0' = a_0 + \Delta a_0' \\ a_{1s}' = a_{1s} + \Delta a_{1s}' \\ b_{1s}' = b_{1s} + \Delta b_{1s}' \end{cases} \quad \ldots (16)$$

The iced-flapping angle of the rotor blade at an arbitrary azimuth angle ψ is

$$\beta' = a_0' - a_{1s}'\mathrm{Cos}\psi - b_{1s}'\mathrm{Sin}\psi \quad \ldots (17)$$

Finally, the iced helicopter dynamic model can be established. By adopting linear perturbation theory[27], the ice-free/iced stability and control derivatives can be calculated to allow consideration of the iced helicopter dynamic characteristics. Figure 1 shows the flow chart describing the calculation of the iced helicopter flight characteristics.

https://doi.org/10.1017/S0001924000007375 Published online by Cambridge University Press

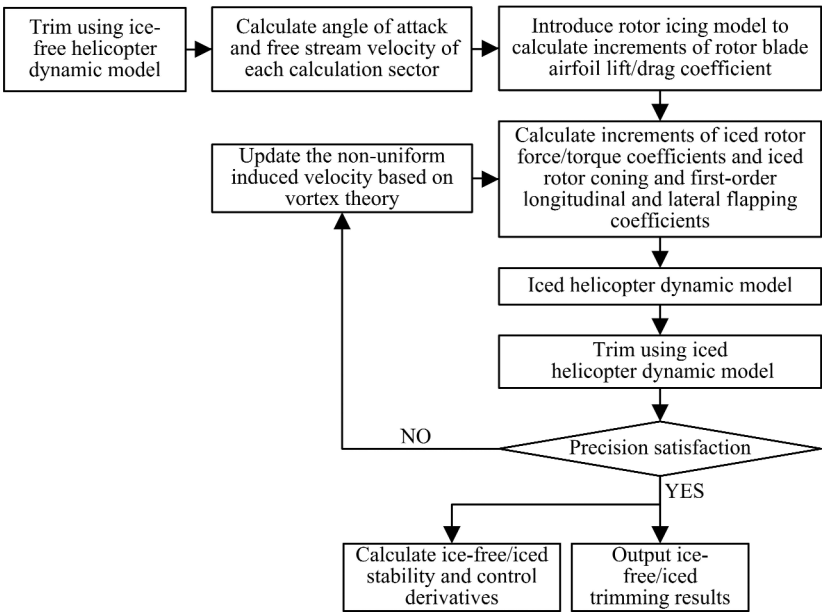


Figure 1. Iced helicopter flight characteristics calculation.

2.3 State-space model

To determine the response of an ice-free/iced helicopter dynamic model to an arbitrary control input, it is necessary to transform the model into a linear state-space representation that will utilise the ice-free/iced stability derivatives. This section establishes that coupled, longitudinal and lateral/directional state-space model using an (x_B, y_B, z_B) body-axis system. Time invariance of the model is assumed. The state-space description of perturbations about a steady-state or trim condition can be given by

$$\begin{cases} \dot{X} = AX + BU \\ Y = CX + DU \end{cases} \quad \ldots (18)$$

The linear equations of motion of this coupled state-space model are defined as Taylor-series expansion

$$\begin{cases} \dot{u} = X_u u + X_v v + X_w w + X_p p + (X_q - w_0)q + (X_r + v_0)r - g\mathrm{Cos}\theta_0\theta + X_{\delta_B}\delta_B + X_{\delta_C}\delta_C + X_{\delta_S}\delta_S + X_{\delta_R}\delta_R \\ \dot{v} = Y_u u + Y_v v + Y_w w + (Y_p + w_0)p + Y_q q + (Y_r - u_0)r - g\mathrm{Sin}\theta_0\mathrm{Sin}\phi_0\theta + g\mathrm{Cos}\theta_0\mathrm{Cos}\phi_0\phi + Y_{\delta_B}\delta_B + Y_{\delta_C}\delta_C + Y_{\delta_S}\delta_S + Y_{\delta_R}\delta_R \\ \dot{w} = Z_u u + Z_v v + Z_w w + (Z_p - v_0)p + (Z_q + u_0)q + Z_r r - g\mathrm{Sin}\theta_0\mathrm{Cos}\phi_0\theta - g\mathrm{Cos}\theta_0\mathrm{Sin}\phi_0\phi + Z_{\delta_B}\delta_B + Z_{\delta_C}\delta_C + Z_{\delta_S}\delta_S + Z_{\delta_R}\delta_R \\ \dot{p} = L_u u + L_v v + L_w w + L_p p + L_q q + L_r r + I_{xz}\dot{r}/I_{xx} + L_{\delta_B}\delta_B + L_{\delta_C}\delta_C + L_{\delta_S}\delta_S + L_{\delta_R}\delta_R \\ \dot{q} = \mathrm{M}_u u + \mathrm{M}_v v + \mathrm{M}_w w + \mathrm{M}_p p + \mathrm{M}_q q + \mathrm{M}_r r + \mathrm{M}_{\delta_B}\delta_B + \mathrm{M}_{\delta_C}\delta_C + \mathrm{M}_{\delta_S}\delta_S + \mathrm{M}_{\delta_R}\delta_R \\ \dot{r} = N_u u + N_v v + N_w w + N_p p + N_q q + N_r r + I_{xz}\dot{p}/I_{zz} + N_{\delta_B}\delta_B + N_{\delta_C}\delta_C + N_{\delta_S}\delta_S + N_{\delta_R}\delta_R \\ \dot{\phi} = p + \mathrm{Sin}\phi_0\mathrm{Tan}\theta_0 q + \mathrm{Cos}\phi_0\mathrm{Tan}\theta_0 r \\ \dot{\theta} = \mathrm{Cos}\phi_0 q - \mathrm{Sin}\phi_0 r \\ \dot{\psi} = \mathrm{Sin}\phi_0\mathrm{Sec}\theta_0 q + \mathrm{Cos}\phi_0\mathrm{Sec}\theta_0 r \end{cases} \quad \ldots (19)$$

https://doi.org/10.1017/S0001924000007375 Published online by Cambridge University Press

The coupled equations assume steady, level flight at 1g, trimmed so that in the body-axis system $p_0 = q_0 = r_0 = 0$. The equations can be decoupled by pre-multiplying by the mass matrix **E**:

$$\mathbf{E} = \begin{bmatrix} 1 & 0 & 0 & 0 & 0 & 0 & 0 & 0 & 0 \\ 0 & 1 & 0 & 0 & 0 & 0 & 0 & 0 & 0 \\ 0 & 0 & 1 & 0 & 0 & 0 & 0 & 0 & 0 \\ 0 & 0 & 0 & 1 & 0 & -I_{xz}/I_{xx} & 0 & 0 & 0 \\ 0 & 0 & 0 & 0 & 1 & 0 & 0 & 0 & 0 \\ 0 & 0 & 0 & -I_{xz}/I_{zz} & 0 & 1 & 0 & 0 & 0 \\ 0 & 0 & 0 & 0 & 0 & 0 & 1 & 0 & 0 \\ 0 & 0 & 0 & 0 & 0 & 0 & 0 & 1 & 0 \\ 0 & 0 & 0 & 0 & 0 & 0 & 0 & 0 & 1 \end{bmatrix} \quad \ldots (20)$$

such that

$$X = [u \quad v \quad w \quad p \quad q \quad r \quad \theta \quad \phi \quad \psi]^T \quad \ldots (21)$$

where the plant matrix is now transformed into the decoupled form $\mathbf{E}^{-1}\mathbf{A}$. The corresponding control distribution matrix is now represented as $\mathbf{E}^{-1}\mathbf{B}$. The state and control vectors are represented by

$$X = [u \quad v \quad w \quad p \quad q \quad r \quad \theta \quad \phi \quad \psi]^T \quad \ldots (22)$$

$$U = [\delta_B \quad \delta_C \quad \delta_S \quad \delta_R]^T \quad \ldots (23)$$

Based upon the normal coupled longitudinal and lateral/directional state-space model of Equation (21), the ice-free/iced helicopter stability, controllability, and flying qualities can be examined using MATLAB® software.

2.4 Rotor icing conditions

For selecting values of icing-related cloud variables to establish the simulated icing conditions, the 14 CFR, Part 25 and 29, Appendix C icing design envelopes[21] are used in the present work. According to the icing design envelopes, the icing conditions can be classified as 'continuous maximum' and 'intermittent maximum' conditions. 'Continuous maximum' conditions represent a portion of stratiform icing conditions or layer-type clouds. And 'intermittent maximum' conditions represent a portion of convective, or cumuliform, clouds and icing conditions.

Based on the icing design envelopes converted to a distance-based format[21], the probable maximum (99%) value of cloud liquid water content (LWC_{max}) can be expected as an average over a specified reference distance (i.e. cloud horizontal extent, *HE*), for a given atmospheric temperature (T_S) and median volumetric diameter (*MVD*) in the cloud. Furthermore, the *HE* in cumuliform and stratiform clouds should be, respectively, restricted from 0·26 to 5·0 nautical miles and from 5 to 300 nautical miles. In this paper, works mainly focus on the flight characteristics in icing environments encountered in cumuliform clouds ('intermittent maximum' conditions). For a helicopter rotor icing problem, *HE* can be written as

https://doi.org/10.1017/S0001924000007375 Published online by Cambridge University Press

Table 1
Simulated icing conditions (cumuliform clouds)

IC	①	②	③	④	⑤	⑥	⑦
$\dot{X}$	[0, 120]	[0, 120]	[0, 120]	[0, 120]	[0, 120]	30	30
τ	2	2	2	2	2·5	3	3
HE_{max}	4	4	4	4	5	1·5	1·5
LWC_{max}	1·539	0·894	1·539	1·041	1·462	1·101	1·101
LWC	0·8	0·8	1·2	0·8	0·8	0·5	0·4,0·6,0·8
T_S	–20·0	–30·0	–20·0	–20·0	–20·0	–12,–15,–25,–30	–30
MVD	20	20	20	25	20	20	20

IC	⑧	⑨	⑩	⑪	⑫	⑬	⑭
$\dot{X}$	30	30	30	30	40	40	40
τ	3	2,4,6	2,4,6	2,4,6	6	6	6
HE_{max}	1·5	3	3	3	4	4	4
LWC_{max}	0·794	2·023	1.369	1.175	0·894	0·645	0·894
LWC	0·5	0·75,1·00,1·25	0·5	0·5	0·5,0·75	0.5	0·75
T_S	–30	–20·0	–20·0	–20,–25,–30	–30	-30	–20,–25,–30
MVD	6,15,20,25	20	15,20,25	20	20	15, 25	20

$$HE = \dot{X} \cdot \tau / 60 \qquad \ldots (24)$$

Because LWC_{max} is inversely proportional to HE[21], the LWC_{max} can be determined directly by referring the intermittent maximum LWCs converted to distance-adjusted values[21], once the T_S, MVD, and HE_{max} were chosen. Table 1 gives the rotor icing conditions which are in accord with intermittent maximum (cumuliform clouds) atmospheric icing conditions.

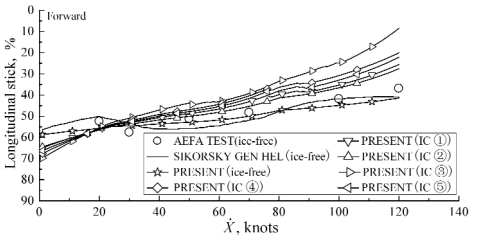
3.0 TRIM, STABILITY, AND CONTROLLABILITY

Using the helicopter dynamic model described in preceding section, flight characteristics for a UH-60A helicopter are investigated for forward flight. Present works mainly focus on the flight characteristics in icing environments encountered in cumuliform clouds as described in Table 1.

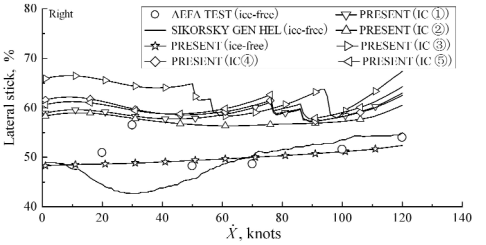
3.1 Trim characteristics

As Fig. 2 indicates, the trim data calculated with the ice-free helicopter model, the AEFA TEST[28], and the Sikorsky GEN HEL model[28] are in good agreement with the exception of some discrepancies in the low-speed flight, which suggest that the ice-free helicopter dynamic model created is both feasible and effective, and can be employed to further study the effects of icing on flight dynamic characteristics of the chosen vehicle. Actually, tail rotor operation is strongly influenced by the presence of the main rotor wake and the downstream turbulence from the main rotor hub. However, because different flight conditions have different complex influence of rotor wash/tail interaction, the aerodynamic interactions between the main rotor and tail rotor in low-speed flight are the most severe and the hardest to predict[29]. The present work has not found

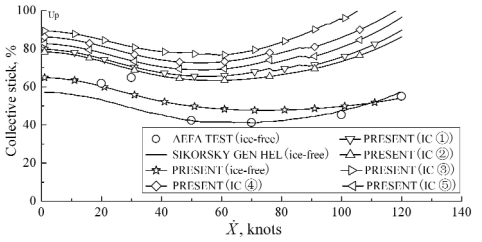
https://doi.org/10.1017/S0001924000007375 Published online by Cambridge University Press



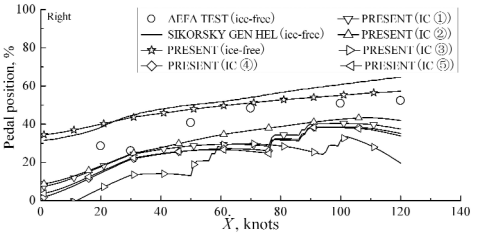
(a) Longitudinal control stick.



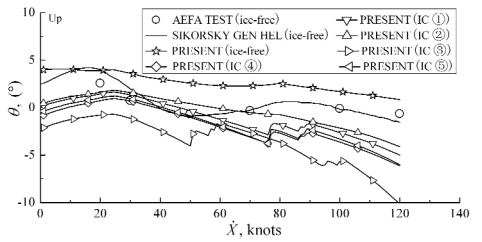
(b) Lateral control stick.



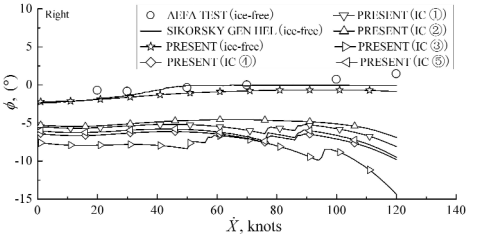
(c) Collective control stick



(d) Pedal position.



(e) Pitching attitude angle



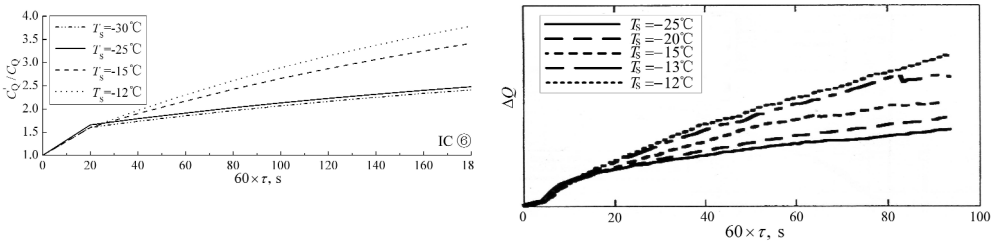
(f) Rolling attitude angle.

Figure 2. Trim curves and attitude angles.

an effective method to model the whole rotor wash/tail interactions in the full forward flight range and then inevitably resulted in some discrepancies in the low-speed flight.

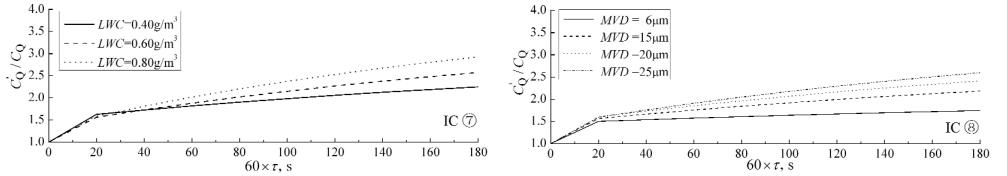
Figure 2 preliminarily confirms the iced trim characteristics observed in Ref. 11. Present works focus on characteristics due to the variation of icing time, atmospheric temperature, liquid water content, and median volumetric diameter (icing conditions are from IC ① to ⑤). It is indicated that the liquid water content is seen to have the most serious effect upon trim characteristics, with median volumetric diameter placing second in this category. A decrease in atmospheric temperature ($T_S \leq -25$ºC) tends to reduce the effect of icing upon control stick trim states as compared to the ice-free states, although the effects are small. Furthermore, because of blade natural ice shedding and high local temperature on the blade surface ($T_C \geq 0$ºC), the lateral stick, pedal position, and pitch/roll attitudes exhibit a trend to revert to the ice-free trim state at some flight velocities. It can be concluded that ice shedding and variations in local temperature on the blade surface affect mainly lateral/directional trim characteristics and vehicle attitude. It can

https://doi.org/10.1017/S0001924000007375 Published online by Cambridge University Press



(a) Present results (b) Icing tunnel test data [6]

Figure 3. Rotor torque rise trend with T_S.



(a) Rotor torque rise trend with LWC (b) Rotor torque rise trend with MVD

Figure 4. Rotor torque rise trend with *LWC* and *MVD*.

be conjectured that the reason for this is that ice shedding or high local temperature ($T_C \geq 0$ºC) first occurs on the rotor-blade tip at an azimuth angle of $\psi = 90$º.

Figure 3(a) shows the effect of temperature upon the relative rotor torque coefficient (C'_Q/C_Q). The icing condition is identified as IC ⑥. Figure 3(b) is the corresponding icing tunnel test data[8]. From Fig. 3 it is seen that the effect of atmospheric temperature upon the relative rotor torque coefficient shows a similar trend with icing time for both the present model and the icing tunnel tests, a further validation of the iced helicopter model developed herein. In addition, during the process of the completing the rotor icing calculation of shown in Fig. 3(a), it was found that the –30ºC and –25ºC curves were clearly a result of rime ice, while the –15ºC and –12ºC curves were glaze, just as in the icing tunnel test [9]. And it is very obvious that the glaze ice accretion has more severe effect upon rotor torque than the rime ice accretion with the increase of the icing time. Corresponding studies on the effects of icing on rotor torque in terms of liquid water content and median volumetric diameter (the icing conditions are identified as ICs ⑦ and ⑧, respectively) are also summarised in Fig. 4. Both Figs 3 and 4 reveal that the atmospheric temperature, liquid water content, and median volumetric diameter each have severe and potentially hazardous effects upon rotor torque.

3.2 Stability

The study is now extended to an investigation of helicopter stability due to icing. Tables 2 and 3 show the representative UH-60A stability roots in ice-free and five of the iced conditions in Table 1 (from IC ① to ⑤). It can be concluded that the modal characteristics of the dynamic modes are not changed except for some changes in the roots, themselves. Furthermore, rotor icing tends to reduce the stability of the longitudinal and lateral/directional oscillatory modes.

https://doi.org/10.1017/S0001924000007375 Published online by Cambridge University Press

Table 2
Longitudinal stability roots

IC	ice-free	①	②	③	④	⑤
$\dot{X}$ = 40knots	–0·2496±0.0841*j* –0·7678, 0·1149	–0·1136±0.2215*j* –1·0922, 0·1750	–0·1211±0·2259*j* –1·0805, 0·1818	–0·0031±0·1754*j* –1·2144, 0·0742	–0·0637±0·2047*j* –1·1604, 0·1355	–0·0930±0·2172*j* –1·1283, 0·1673
$\dot{X}$ = 80knots	–0·7956±0·8857*j* –0·0108±0·1290*j*	–0·7763±0·5594*j* –0·0143±0·1308*j*	–0·7801±0·6006*j* –0·0140±0·1317*j*	–0·7909±0·1957*j* –0·0026±0·1883*j*	–0·7828±0·4040*j* –0·0110±0·1707*j*	–0·7771±0·4850*j* –0·0133±0·1499*j*

Table 3
Lateral/directional stability roots

IC	ice-free	①	②	③	④	⑤
	–0·0683±1·1900*j*	–0·0322±1·3584*j*	–0·0523±1·3286*j*	0·0579±1·4809*j*	0·0013±1·4149*j*	-0·0144±1·3827*j*
$\dot{X}$ = 4 knots	–3·7687, –0·0586 0	–4·1770, –0·0900 0	–4·0790, –0·0798 0	–4·132, –0·1257 0	–4·4018, –0·1032 0	–4·2783, –0·0967 0
	–0·0927±1·6892*j*	0·0959±1·.8656*j*	0·0557±1·8336*j*	0·2010±2·0095*j*	0·1630±1·9254*j*	0·1364±1·8978*j*
$\dot{X}$ = 80knots	–3·9251, –0·0272 0	–4·5211, –0·0569 0	–4·4299 ,–0·0506 0	–4·9854, –0·0725 0	–4·7826, –0·0639 0	–4·6509, –0·06150 0

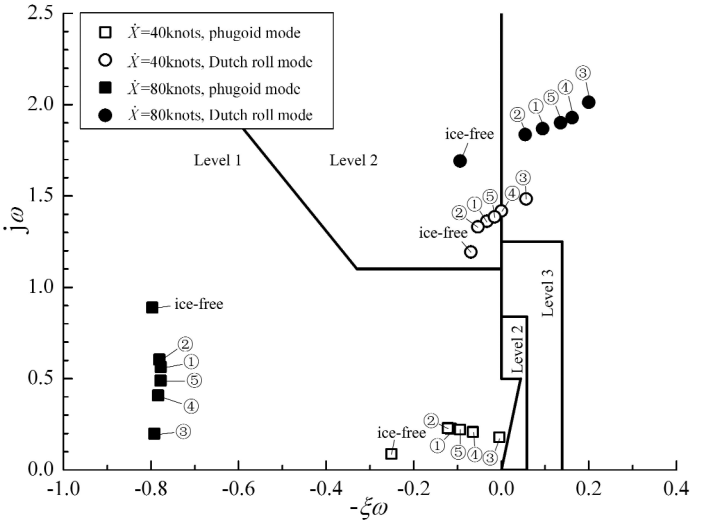


Figure 5. Effects of icing on dynamic response.

Figure 5 shows the effects of icing upon helicopter dynamic response as quantified in MIL-F-8330[(22)]. It can be concluded that the effects of icing on the Dutch roll mode are more serious than on the phugoid mode. Different icing conditions have different effects upon helicopter stability characteristics. An increase in liquid water content has the most serious effect on stability as compared to the variations in atmospheric temperature and median volumetric diameter. Nevertheless, an increase in icing time always decreases stability, especially that of the Dutch roll mode.

https://doi.org/10.1017/S0001924000007375 Published online by Cambridge University Press

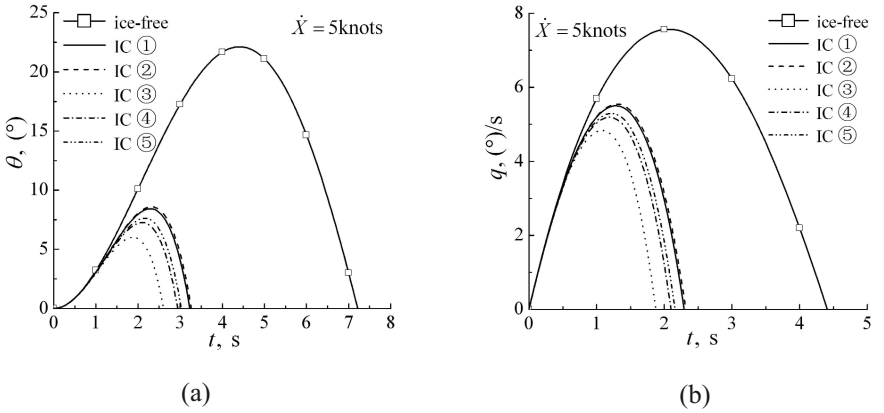


Figure 6. Effects of icing on responses of θ and q.

3.3 Controllability

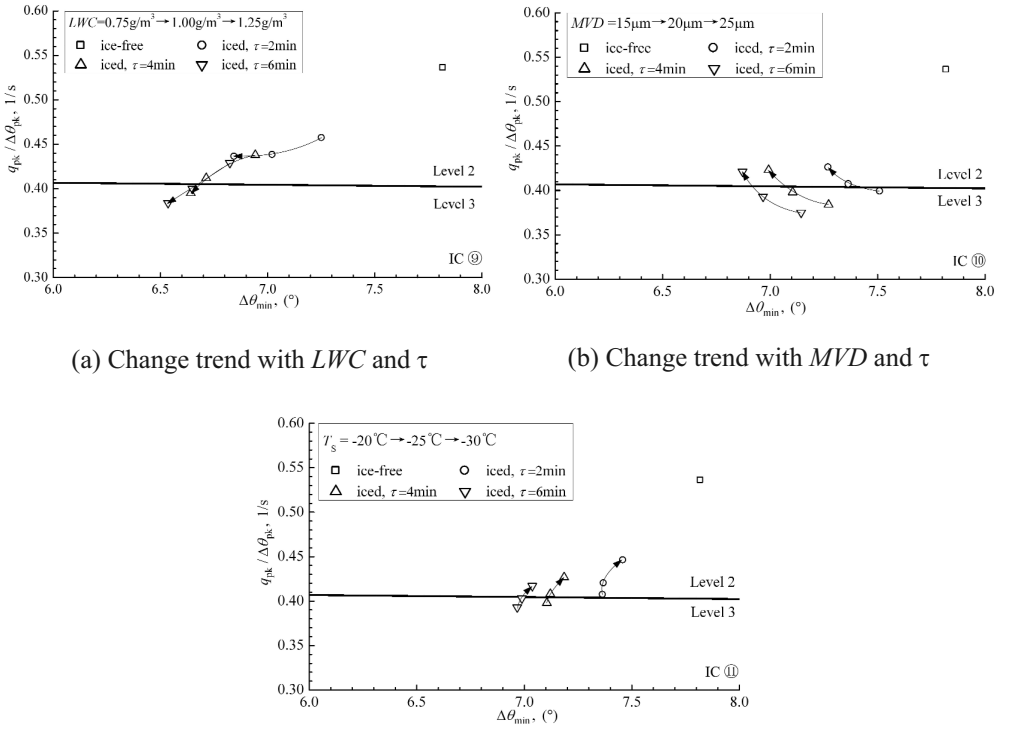
According to MIL-F-8330, the controllability of the helicopter can be assessed by investigating control power and control sensitivity. The consideration of prescribed attitude changes that must occur within 1·0 second of abrupt application of pitch, roll and yaw commands (i.e., multiple control inputs in the most critical combination) with the wind from the most critical direction relative to the helicopter can be used as a quantitative measure of minimum control power needs. In addition, an allowable range of control sensitivities can be specified in indirect fashion in terms of the attitude response within 1·0sec for a single control input. Two indices of assessing controllability can be obtained through pitch/roll/yaw attitude response. Here, a 1·0cm step longitudinal/lateral/directional control input is employed in order to predict the effects of icing on helicopter controllability.

Helicopter controllability from IC ① through ⑤ are examined next. Figure 6 shows the effects of icing on helicopter pitch-attitude and pitch-rate responses at a forward velocity of $\dot{X}$ = 5knots. Referring to Fig. 6, conclusions can be drawn as follows: At 5 knots forward velocity, rotor icing reduces the peak value of pitch-attitude and pitch-rate responses. Referring to the time histories for the five icing conditions, an increase in liquid water content is seen to have the most serious effect upon controllability. It also shows that the response of the helicopter in IC ② tends to revert to the ice-free response but the icing effects due to variation in atmospheric temperature are small. The increase in median volumetric diameter also has serious effects upon control response. Basically, these trends are similar to the effects of icing on stability.

4.0 FLYING QUALITIES

Referring now to ADS-33E-PRF, and using the ice-free/iced helicopter state-space model, the metrics of attitude quickness, interaxis coupling and vertical axis control power are examined in terms of icing time, and the three icing-related cloud variables.

https://doi.org/10.1017/S0001924000007375 Published online by Cambridge University Press



(a) Change trend with *LWC* and τ

(b) Change trend with *MVD* and τ

(c) Change trend with T_S and τ

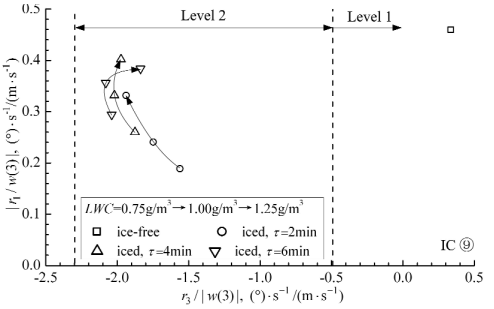
Figure 7. Effects of icing on pitch attitude quickness.

4.1 Attitude quickness

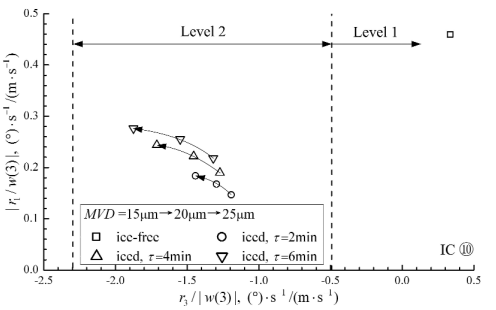
Attitude quickness is one of the more important metrics in the study of helicopter flying qualities. This metric quantifies the transient characteristics of the maneuver and the validity of the helicopter response to a control command. According to ADS-33E-PRF, the required attitude changes shall be made as rapidly as possible from one steady attitude to another without significant reversals in the sign of the cockpit control input relative to the trim position. Taking the pitch channel as an example, attitude quickness can be defined as the ratio of peak pitch rate to the change in pitch attitude, $q_{pk}/\Delta\theta_{pk}$. At identical values of the minimum attitude change, the greater this ratio, the better the attitude quickness. A 1·0cm pulsive longitudinal control input is used herein (the action time is 1·0sec). Results are shown in Fig. 7 where the bold solid line represents the Level 2/Level 3 boundary for target acquisition and tracking.

Figure 7 allows conclusions to be drawn as follows: Rotor icing degrades the flying qualities associated with pitch-attitude quickness. With an increase in icing time, indices of attitude quickness indicate a reduction in flying qualities. An increase in liquid water content also degrades flying qualities. An increase in median volumetric diameter would appear to improve flying qualities slightly. A decrease in atmospheric temperature ($T_S \leq -25$ºC) also results in a slight improvement in flying qualities. This is probably attributable to creation of a smoother icing surface on the blade in very low atmospheric icing conditions.

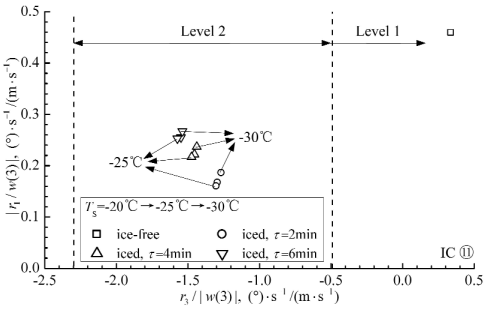
https://doi.org/10.1017/S0001924000007375 Published online by Cambridge University Press



(a) Change trend with *LWC* and τ



(b) Change trend with *MVD* and τ



(c) Change trend with T_S and τ

Figure 8. Effects of icing on yaw due to collective coupling.

4.2 Interaxis coupling

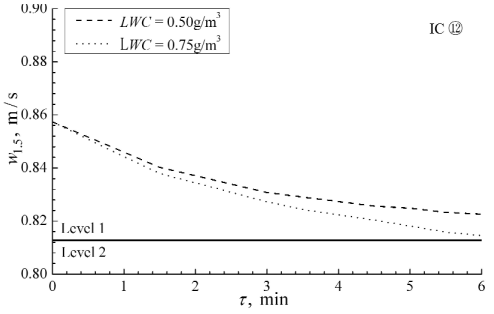
Referring again to ADS-33E-PRF, control inputs to achieve a desired response in one axis shall not result in objectionable responses in or more of the other axes. There are three aspects for assessing interaxis coupling, yaw due to collective for aggressive agility, pitch due to roll, and roll due to pitch for aggressive agility and for target acquisition and tracking. Here, the ice-free/iced yaw due to collective in terms of icing time, atmospheric temperature, liquid water content, and median volumetric diameter are analysed in detail. The $|r_1/w(3)|$ and $|r_3/w(3)|$ in Fig. 8 are yaw due to collective coupling indices, where $w(3)$ is the vertical velocity at t = 3 seconds, r_1 is the first yaw-rate peak before 3·0 seconds or the yaw rate $r(1)$ at t = 1 second. If no peak occurs before t = 3 seconds, r_3 can be written as:

$$r_3 = \begin{cases} r(3) - r_1 & r_1 > 0 \\ r_1 - r(3) & r_1 < 0 \end{cases} \quad \ldots (25)$$

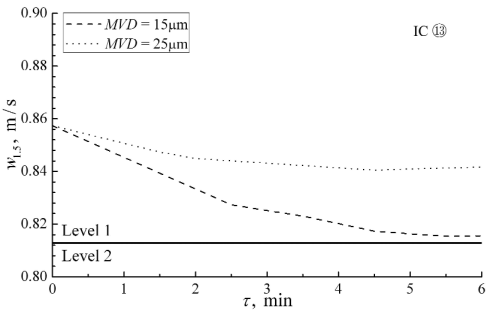
where $r(3)$ is the yaw rate at t = 3 seconds.

Here a 1·0 cm step collective control input is employed to determine icing effects on yaw due to collective coupling. Results are shown in Fig. 8. Figure 8 allows conclusions to be drawn as follows: With an increase in icing time, indices of yaw due to collective coupling tend to degrade. At similar icing times, higher liquid water content degrades the flying qualities associated with

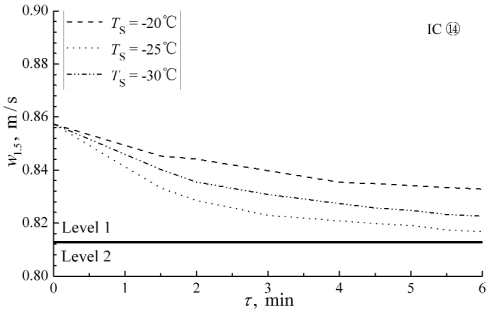
https://doi.org/10.1017/S0001924000007375 Published online by Cambridge University Press



(a) Change trend with *LWC* and τ



(b) Change trend with *MVD* and τ



(c) Change trend with T_S and τ

Figure 9. Effects of icing on vertical axis control power.

yaw due to collective coupling. For $T_S \leq -25$ºC, the lower the atmospheric temperatures, the slightly better are the corresponding flying qualities associated with yaw due to collective coupling. This again is probably attributable to creation of a smoother icing surface on the blade in very low atmospheric icing conditions.

4.3 Vertical axis control power

Vertical axis control power is also one of the more important metrics in the study of helicopter flying qualities. Referring again to ADS-33E-PRF, it can be quantified as a specified vertical rate achieved 1·5 second after initiation of a rapid displacement of the collective control from trim. Here, a 1·0cm collective control input is employed to determine icing effects on vertical axis control power. Results are shown in Fig. 9 and conclusion can be drawn as follows: Liquid water content has a more severe effect on the vertical axis power as compared with median volumetric diameter and atmospheric temperature. With an increase in liquid water content, the vertical axis control power degrades significantly at similar icing times, as can be seen in Fig. 9(a). Furthermore, the effects of icing on vertical axis control power due to MVD exhibits the same trend as the effect of icing on interaxis coupling, as shown in Fig. 8(b) and Fig. 9(b). In addition, –30ºC atmospheric temperature makes the flying qualities slight better than that at –25ºC, as can be seen in Fig. 9(c).

https://doi.org/10.1017/S0001924000007375 Published online by Cambridge University Press

5.0 CONCLUSIONS

Compared with previous icing studies[11], present work mainly aims at: (*i*) considering different types of ice accretion due to local temperature variations on the blade surface to study rotor icing in detail, (*ii*) incorporating the iced-rotor flapping model to improve the iced helicopter dynamic model, (*iii*) selecting values of icing-related cloud variables to establish the simulated icing conditions based on the 14 CFR, Part 25 and 29, Appendix C icing design envelopes, and (*iv*) developing a coupled longitudinal and lateral/directional state-space model to evaluate the effects of icing on stability and a limited set of flying qualities metrics under the icing conditions in accord with the 14 CFR, Part 25 and 29, Appendix C icing design envelopes. Based upon the results obtained, the following conclusions can be summarised:

1. Liquid water content has the most serious effect upon helicopter flight characteristics, with median volumetric diameter placing second in this category. And a decrease in atmospheric temperature ($T_S \leq -25$ºC) has a trend to reduce the effect of icing upon control stick trim states as compared to the ice-free states.
2. Different types of ice accretion have different effects on rotor torque characteristics. In detail, the glaze ice accretion has more severe effect upon rotor torque than the rime ice accretion with the increase of the icing time. Besides, effects of icing on stability have the same change trend as the trim characteristics in the five icing conditions (from IC ① to ⑤).
3. An examination of helicopter flying qualities indicates that the severity of ice accretions on helicopter rotor blades is highly dependent upon the variation of the three icing-related cloud variables. An increase in liquid water content makes the attitude quickness, the yaw due to collective coupling, and the vertical axis control power have a trend of degradation. A decrease in atmospheric temperature ($T_S \leq -25$ºC) makes the three flying qualities metrics degrade more slowly.

REFERENCES

1. ENDERS, J.H., HILSENROD, A. and SIBERT, L.C.G.W. Aircraft icing, 1978, FAA-RD-78-109.
2. BRAGG, M.B. and GREGOREK, G.M. An analytical approach to airfoil icing, 1981, AIAA 1981-0403, 19th Aerospace Sciences Meeting, 12-15 January 1981, St Louis, MO, USA.
3. BRAGG, M.B. and GREGOREK, G.M. Aerodynamic characteristics of airfoils with ice accretion, AIAA 1982-0282, 20th Aerospace Sciences Meeting, 11-14 January 1982, Orlando, FL, USA.
4. KORKAN, K.D., DADONE, L. and SHAW, R.J. Performance degradation of propeller systems due to rime ice accretion, *J Aircr*, 1984, **21**, (1), pp 44-49.
5. KORKAN, K.D., DADONE, L. and SHAW, R.J. Performance degradation of helicopter rotor in forward flight due to ice, *J Aircr*, 1985, **22**, (8), pp 713-718.
6. KORKAN, K.D., DADONE, L. and SHAW, R.J. Helicopter rotor performance degradation in natural icing encounter, *J Aircr*, 1984, **21**, (1), pp 84-85.
7. KORKAN, K.D., CROSS, E.J.J. and MILLER, T.L. Performance degradation of a model helicopter main rotor in hover and forward flight with a generic ice shape, *J Aircr*, 1984, **21**, (10), pp 823-830.
8. FLEMMING, R.J. and LEDNICER, D.A. High speed ice accretion on rotorcraft airfoils, 1985, NASA CR 3910.
9. FLEMMING, R.J., RANDALL, K.B. and THOMAS, H.B. Role of wind tunnels and computer codes in the certification and qualification of rotorcraft for flight in forecast icing, 1994, NASA TM-106747.
10. FLEMMING, R.J. and LUSZCZ, M.T. Incorporation of an empirical icing code in a flight simulator, 2003, SAE 2003-01-2104, FAA In-Flight Icing/Ground De-icing International Conference & Exhibition, 16-20 June 2003, Chicago, IL, USA.
11. CAO, Y.H., LI, G.Z. and ZHONG, G. Tandem helicopter trim and flight characteristics in the icing condition, *J Aircr*, 2010, **47**, (5), pp 1559-1569.

https://doi.org/10.1017/S0001924000007375 Published online by Cambridge University Press

12. HANKS, M.L., BENSON, J.O. and DIEKMAN, V.L. Limited artificial and natural icing tests — production UH-60A helicopter (re-evaluation), 1981, USAAEFA Project No. 80-14.
13. ARMAND, C. Aircraft Icing - Techniques and facilities used at the ONERA modane centre for icing tests, 1978, AGARD Advisory Report No 127.
14. GUFFOND, D.P. Icing and de-icing test on a 1/4-scale rotor in the ONERA S1MA wind tunnel, 1986, AIAA 1986-0480, 24th Aerospace Sciences Meeting 6-9 January 1986, Reno, NV, USA.
15. BRITTON, R.K. and BOND, T.H. A review of ice accretion data from a model rotor icing test and comparison with theory, 1991, AIAA 1991-0661, 29th Aerospace Sciences Meeting, 7-10 January 1991, Reno, NV, USA.
16. CAO, Y.H. and CHEN, K. Helicopter icing, *Aeronaut J*, 2010, **114**, (1152), pp 83-90.
17. RUFF, G.A. and BERKOWITZ, B.M. Users manual for the NASA Lewis ice accretion code (LEWICE), 1990, NASA Contractor Report 185129.
18. HEDDE, T. and GUFFOND, D. Improvement of the ONERA 3D icing code, comparison with 3D experiment shapes, 1993, AIAA 1993-0169, 31st Aerospace Sciences Meeting & Exhibition, 11-14 January 1993, Reno, NV, USA.
19. MINGIONE, G., BRANDI, V. and SAPORITI, A. A 3D ice accretion simulation code, 1999, AIAA 1999-0247, 37th Aerospace Sciences Meeting & Exhibition, 11-14 January 1999, Reno, NV, USA.
20. HABASHI, W.G., MORENCY, F. and BEAUGENDRE, H. FENASP-ICE: a second generation 3D CFD-based in-flight icing simulation system, 2003, SAE 2003-01-2157, FAA In-Flight Icing/Ground De-icing International Conference & Exhibition, 16-20 June 2003, Chicago, IL, USA.
21. RICHARD K.J. Icing design envelopes (14 CFR Parts 25 and 29, Appendix C) converted to a distance-based format, 2002, DOT/FAA/AR-00/30.
22. CHALK, C.R., KEY, D.L. and KROLL, J.J. Background information and user guide for MIL-F-83300 military specification flying qualities of piloted V/STOL aircraft, 1971, Cornell Aeronautical Laboratory.
23. UNITED STATES ARMY AVIATION AND MISSILE COMMAND. ADS-33E- PRF Aeronautical design standard, performance specification, handling qualities requirements for military rotorcraft, 2000, Redstone Arsenal Alabama: Aviation Engineering Directorate, AL, USA.
24. FLEMMING, R.J. and LEDNICER, D.A. Correlation of icing relationships with airfoil and rotorcraft icing data, *J Aircr*, 1986, **23**, (10), pp 737-743.
25. JOHNSON, W. *Helicopter Theory*, 1980, Princeton University Press, Princeton.
26. CAO, Y.H., LI, G.Z. and YANG, Q. Studies of trims, stability, controllability, and some flying qualities of a tandem rotor helicopter, Proceedings of the Institution of Mechanical Engineers Part G, *J Aerospace Eng*, 2009, **223**, (G2), pp 171-177.
27. MCRUER, D., ASHKENAS, I. and GRANHAM, D. *Aircraft Dynamics and Automatic Control*, 1973, Princeton University Press, Princeton, USA.
28. BALLIN, M.G. Validation of a real-time engineering simulation of the UH-60A helicopter, 1987, NASA TM-88360.
29. LEISHMAN, J.G. *Principles of Helicopter Aerodynamics*, 2006, Cambridge University Press, Cambridge, UK.

https://doi.org/10.1017/S0001924000007375 Published online by Cambridge University Press